Applied Surface Science 302 (2014) 6–10

Contents lists available at ScienceDirect

Applied Surface Science

journal homepage: www.elsevier.com/locate/apsusc

High-speed laser ablation of metal with pico- and subpicosecond pulses

V.I. Mazhukin*, M.M. Demin, A.V. Shapranov

Keldysh Institute of Applied Mathematics of RAS, 4a Miusskaya sqr, 125047 Moscow, Russia

ARTICLE INFO

Article history:
Received 30 June 2013
Received in revised form 17 January 2014
Accepted 18 January 2014
Available online 28 January 2014

Keywords:
Laser ablation
Pico- and subpicosecond pulses
Homogeneous melting
Heterogeneous melting

ABSTRACT

The mechanism of the high-speed ablation of aluminum with pico- and subpicosecond (10^{-11}–10^{-13} s) laser pulses is considered. Mathematical modeling based on the continuum non-equilibrium two-temperature (TTM) model revealed that in a relatively narrow range of fluence 0.25–0.7 J/cm^2, the regime of mechanical fragmentation of the irradiated surface is realized. The maximum values of the lattice temperature for the specified range of fluence are 2100–3500 K. The removal of the material is mechanical due to the negative stresses in the rarefaction wave following the shock wave. Explicit tracking of temporal and spatial position of the melting front has allowed establishing its role in the generation of superheated metastable states in the solid phase and the propagation of the shock wave. The removed material with total thickness of 60–100 nm is a collection of separate plates with thickness from 1 nm to 55 nm.

1. Introduction

Ultrashort laser action on metals with pulse duration of $\tau_L \approx 10^{-12}$–5×10^{-14} s has the features peculiar only to this range of duration, in particular, the features that appear in the form of a new mechanism of ablation. Thus, while in the region of laser pulses of long duration, $\tau_L \approx 10^{-6}$–10^{-9} s, the main mechanism of material removal is surface evaporation, the dominant mechanism in the pico- and femtosecond range is spall ablation. Removal of material is increased by several orders of magnitude compared to the surface evaporation. It was found [1,2] that usage of large values of fluence $F \approx 1$–10 J/cm^2 results in spallation in solid matter at the rear side of the target. The process is accompanied by great destruction and the substance near the irradiated surface is in the region of supercritical parameters.

Experimental [3] and theoretical [4,5] research allowed to determine a relatively narrow range of fluence $F \approx 0.25$–0.7 J/cm^2, in which the spall ablation due to the unloading phenomena was observed in the melt near the irradiated surface. At that, the irradiated surface is in the subcritical region of parameters. This mechanism of material removal can be the basis for the high-speed ablation. However, complex processes that take place in the irradiated zone and that are associated with the metastable superheated states in the solid phase and homogeneous mechanism of melting were not adequately investigated. Spallation in solid matter has been extensively studied for many years [1,2,4,5], while detailed information on the dynamic fragmentation of liquid emerging after partial or complete melting by the laser, is yet to be determined. Thus, the study of the dynamic fragmentation of laser shock-loaded metals and evaluation of geometrical sizes of the obtained fragments is an important issue for both fundamental and applied science.

Dynamic fragmentation leads to formation of clouds of liquid droplets of melt ejected into the environment at a high speed. The main method of the theoretical study of these processes is the molecular-dynamics simulation [5–7] using atomistic models. Continuous models are used much less frequently [4]. Their application is limited mainly by the lack of possibility of description of homogeneous mechanisms of melting-crystallization. Additional limitations are associated with the computational complexity of determination of spatial location and propagation of the phase fronts that are typical for the processes of heterogeneous melting-solidification because continuous models [4] usually consider phase transitions, shock waves and spallation without usage of adaptive grids and explicit front tracking. In recent years, a number of theoretical studies [8–14] were published which described and studied various aspects of spallation of irradiated surfaces of the metal targets on the basis of continuum models. However, these models did not explicitly formulate and analyze the melting process.

This paper is dedicated to theoretical modeling of fragmentation of aluminum, melted by a picosecond laser pulse, estimation of the number of molten droplets and determination of their sizes.

* Corresponding author. Tel.:+7 4992507986.
E-mail address: vim@modhef.ru (V.I. Mazhukin).

0169-4332/$ – see front matter © 2014 Elsevier B.V. All rights reserved.
http://dx.doi.org/10.1016/j.apsusc.2014.01.111

2. Model

Modeling of melting and fragmentation is based on the use of the non-equilibrium continuum hydrodynamic model [15,16], supplemented with the equation of laser radiation transfer. The absorbed portion $A_{sur}(T_e) = 1 - R_{sur}(T_e)$ of laser pulse intensity $G(t)$ initiates a number of interrelated processes in it with non-linear nature of development. The description of their behavior is accomplished using a system of hydrodynamic equations, two energy balance equations for the electron and phonon subsystems, and the transport equation for the laser radiation. The system of equations is written for the domain with two moving interphase boundaries $\Gamma_{sl}(t)$, $\Gamma_{k\upsilon}(t)$.

$$\left(\begin{array}{c} \dfrac{\partial \rho}{\partial t} + \dfrac{\partial (\rho u)}{\partial x} = 0 \\ \dfrac{\partial (\rho u)}{\partial t} + \dfrac{\partial (\rho u^2)}{\partial x} + \dfrac{\partial p}{\partial x} = 0 \\ \dfrac{\partial (\rho_e \varepsilon_e)}{\partial t} + \dfrac{\partial (\rho_e u \varepsilon_e)}{\partial x} = -\left(p_e \dfrac{\partial u}{\partial x} + \dfrac{\partial W_e}{\partial x} + g(T_e)(T_e - T_{ph}) + \dfrac{\partial G}{\partial x} \right) \\ \dfrac{\partial (\rho_i \varepsilon_{ph})}{\partial t} + \dfrac{\partial}{\partial x}(\rho_i u \varepsilon_{ph}) = -\left(p_{ph} \dfrac{\partial u}{\partial x} + \dfrac{\partial W_{ph}}{\partial x} - g(T_e)(T_e - T_{ph}) \right) \\ \dfrac{\partial G}{\partial x} + \alpha(T_e) G = 0,\ \rho_e = z \dfrac{m}{M} \rho_i, \\ P = P_e(\rho_e, T_e) + P_{ph}(\rho_i, T_{ph}),\ \varepsilon_e = \displaystyle\int C_e(T_e) dT_e,\ \varepsilon_{ph} = \int C_{ph}(T_{ph}) dT_{ph} \end{array} \right)_{k=s,l}, \quad (1)$$

$t > 0, x_0 < x < \Gamma_{sl}(t) < x < \Gamma_{lv}(t)$

$W_e = -\lambda(T_e, T_{ph}) \frac{\partial T_e}{\partial x}$, $W_{ph} = -\lambda(T_{ph}) \frac{\partial T_{ph}}{\partial x}$, $p(\rho, T) = p(\rho_e, T_e) + p(\rho_i, T_{ph})$, $\rho = \rho_e + \rho_i$. The adopted designations: ρ_i is the density of heavy particles, ρ, u, p, ε, T are the density, gas-dynamic velocity, pressure, internal energy, and temperature correspondingly, $\alpha(T_e)$, $R(T_e)$ are the coefficient of volume absorption and surface reflectivity, G is the energy density of laser radiation, W is the heat flow, m, M, z are the electron and ion mass and ion charge, $C_e(T_e)$, $C_{ph}(T_{ph})$, $\lambda_e(T_e, T_{ph})$, $\lambda_{ph}(T_{ph})$ are the electron and phonon specific heat and thermal conductivity, $g(T_e)$ is the electron–phonon coupling factor. The indexes s,l,υ denote that the value belongs to either solid, liquid or vapor phases, e, ph denotes the electron or phonon gas.

3. Models of heterogeneous melting and evaporation

The model of heterogeneous melting describes processes at the interface solid–liquid under the conditions of significant violation of local thermodynamic equilibrium that are typical for ultrashort laser action. The electron component is assumed to be continuous at the phase boundary relative to the electron density N_e and electron temperature T_e: $W_{e,s} = W_{e,l}$, $T_{e,s} = T_{e,l}$.

The model of heterogeneous melting consists of the system of equations expressing the three conservation laws for the phonon component: mass, momentum, and energy, supplemented with the kinetic condition for the velocity of the melting υ_{sl}:

$$x = \Gamma_{sl}(t) : \rho_s(u_s - \upsilon_{sl}) = \rho_l(u_l - \upsilon_{sl}) \quad (2)$$

$$p_s + \rho_s(u_s - \upsilon_{sl})^2 = p_l + \rho_s(u_s - \upsilon_{sl})^2 \quad (3)$$

$$\left(\lambda \frac{\partial T}{\partial x} \right)_s - \left(\lambda \frac{\partial T}{\partial x} \right)_l = \rho_s L_m^{ne} \upsilon_{sl} \quad (4)$$

$$\upsilon_{sl}(\Delta T_{sl}) = \frac{af}{\lambda} \left(\frac{3 k_B T_{sl}}{m} \right)^{1/2} \left(1 - \exp\left(\frac{L_m(T_m)}{k_B T_m(p_s)} \frac{\Delta T_{sl}}{T_{sl}} \right) \right) \quad (5)$$

The introduction of additional condition (5) is caused by the fact that in addition to the thermodynamic nonequilibrium, phase transitions of the first kind contain kinetic nonequilibrium associated with the molecular-kinetic processes at the interface. For melting-solidification, the kinetic nonequilibrium is characterized by the velocity of interphase boundary υ_{sl}, taking into account the deviation of the phase transition temperature T_{sl} from the equilibrium temperature $T_{m,0}$, i.e. the value of superheating or undercooling. The significant deviation from the equilibrium temperature makes it inacceptable to use the phenomenological condition of constant temperature at the interface $T_{sl} = T_{m,0}$ that is used in the classical type of the Stefan problem. Strictly speaking, the equality $T_{sl} = T_{m,0}$ corresponds to the equilibrium of the two phases of solid–liquid and can be used for very slow phase transitions [16] close to the equilibrium curve. For the fast phase transitions, it is more consistent to replace the phenomenological conditions with the expression for the velocity υ_{sl} obtained from the molecular-kinetic theory [17], [18]. This expression is the main characteristic of the process of melting-crystallization. The designations that are used in (2)–(5): $L_m(T_m(p_s)) = 8897 + 6.374 \times (T_m(p_s) - 925)$ [J/Mole] is the temperature dependence of the equilibrium melting heat, $T_m(p_s) = T_{m,0} + k\, p_s$ is the equilibrium melting curve, $L_m^{ne} = L_m(T_m(p_s)) + \Delta C \Delta T_{sl} + (u_s - u_l)^2(\rho_s + \rho_l)/[2(\rho_s - \rho_l)]$ is the nonequilibrium heat of melting, $\Delta C = (C_s - C_l)$, $\Delta T_{sl} = T_{sl} - T_m(p_s)$, k is a constant, λ is the mean free path, m is the atom mass, a is the interatomic distance, f is the efficiency coefficient–the amount of atoms that remain in solid when passing through the boundary, k_B is the Boltzmann constant.

The approximation of the Knudsen layer is generally used in the current models of heterogeneous evaporation (see [19], and references therein). The main limitation to their use is that acceptable quantitative description of the processes is achieved far from the critical state of matter. Given that the processes of heterogeneous evaporation are well described and investigated over the past decade, its mathematical formulation is not given in the present paper. The modified model of D. Crout was used in the calculations [19].

Complete description of the models of heterogeneous melting and evaporation can be found in Ref. [15].

In metals, the laser radiation is absorbed by free (collectivized) electrons via the inverse bremsstrahlung. Temporal profile of USLP of a Ti:Sapphire laser with wavelength $\lambda_L = 0.8$ μm is approximated by the Gaussian dependence $G = G_0 \exp(-(t/\tau_L)^2)$, where τ_L is the pulse half-width, G_0 is the maximum value of intensity. The value of intensity at the irradiated surface is $G_{sur}(t) = A_{sur}(T_e) G_0(t) \exp(-(t/\tau_L)^2)$, where $A_{sur}(T_e) = 1 - R_{sur}(T_e)$ is the surface absorptance. Propagation of laser radiation deep into the strongly absorbing condensed medium is described by the equation of laser radiation transfer from the system (1), the integration of which leads to Lambert–Beer law.

A modified equation of state $P(\rho, T)$ from Ref. [20] was used in the calculations. The modification was to exclude from consideration the mixed zone solid + liquid.

4. Computational algorithm

The differential model (1)–(2) was approximated by a family of implicit conservative finite difference schemes written on dynamically adapted grids [21]. The method is based on the idea of using an arbitrary non-stationary coordinate system, which allows, in contrast to Euler and Lagrange variables, to perform calculations with an arbitrary number of discontinuous solutions such as shock waves, propagating phase and temperature fronts, contact boundaries and spalled fragments. The algorithm for calculating of a single spall fragment is as follows. The compression wave caused by heating and thermal expansion of the target material is followed by a rarefaction wave with negative pressure that moves from the irradiated surface into the bulk target. If the rarefaction wave meets the spallation criteria for the values of negative pressure, duration and strain rate [22], there may be a mechanical breakaway in this area, i.e., formation of voids in the target material. As a result of spallation, the fragments of matter are separated from the target and move in the direction opposite to the laser pulse. At this, two new moving boundaries are introduced into the point of spallation. If the temperature is high enough, $T > T_b$, saturated vapor is placed between them with appropriate boundary conditions written at the two boundaries for surface evaporation and condensation. In the regimes of laser action where the temperature at the points of the mechanical spallation is not too high, $T < T_b$, it is possible to replace saturated vapor with vacuum for simplicity and without decreasing of the accuracy of the calculations. In this case, we write at the new borders the boundary conditions for the contact discontinuity of condensed medium and vacuum. In addition to the criterion of spallation, we also introduced an additional constraint: the minimum size of the spalled material should not be less than 1 nm, i.e., several atomic layers. A detailed computational grid with increasing concentration of the grid nodes from the center to the both boundaries of the spalled piece is automatically generated in the new domain. Density and temperature remain the same inside the new domain as they were immediately prior to the spallation.

5. Results and discussion

An ultra-short laser pulse with wavelength $\lambda_L = 0.8\ \mu m$ and Gaussian temporal profile $G = G_0 \exp(-(t/\tau)^2)$ with duration $\tau_L = 0.1$ ps and maximum intensity $G_0 = 2.26 \times 10^{12} W/cm^2$ hits the surface of an aluminum target. This value of intensity corresponds to the fluence value of $F = 0.4 J/cm^2$ F. The absorbed threshold fluence of spallation in our computations is about $0.06\ J/cm^2$. The temperature dependence of optical properties $R(T_e)$ and $\alpha(T_e)$ were determined via Fresnel formulas using real and imaginary parts of longitudinal dielectric permittivity. The permittivity of degenerate electron plasma of metal was determined from the numerical solution of the kinetic equation. The methods of determining the optical characteristics of metals and the method of solving the kinetic equation are given in Ref. [23]. The temperature dependencies of $R(T_e)$ and $\alpha(T_e)$ were taken from there and have the form [15]. The absorbed fluence in our computation was about $0.088\ J/cm^2$.

Temporal evolution of the processes in the target is conveniently represented in the form of two consecutive stages: non-equilibrium thermodynamic one with $T_e \gg T_{ph}$ and hydrodynamic one with $T_e \sim T_{ph}$. The first stage includes the release of the laser pulse energy in the electron component and its rapid heating to high temperatures in the subsurface region with $T_{e,max} \approx 1.4 \times 10^4 K$. Slow exchange between the electronic component and the lattice leads

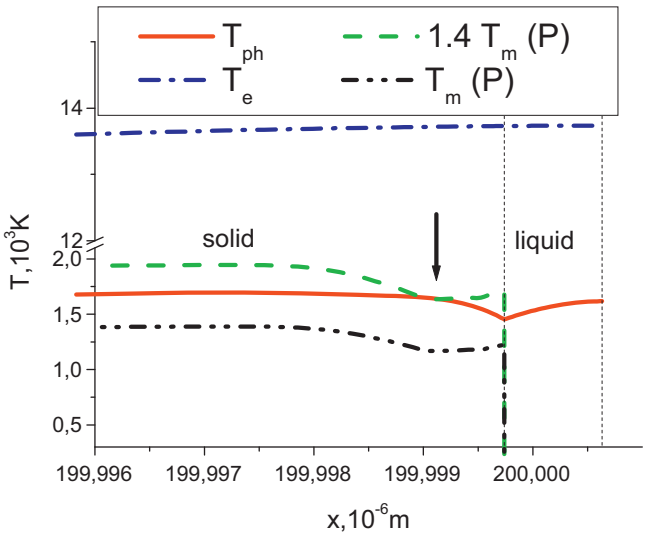

Fig. 1. Start of volume melting at $t = +0.4$ ps. The vertical arrow shows the point of introduction of a new liquid phase.

to a large separation of the electron temperature from the temperature of the phonons, $T_e \gg T_{ph}$, Fig. 1. Melting of the target starts from the irradiated surface with large delay relative to the duration of the laser pulse $t \sim +0.5$ ps. Significant superheating of the melting surface and large spatial temperature gradients provide high propagation velocities for the melting front with the values of about 2.5 km/s. The powerful flow of the material through the phase boundary Γ_{sl} together with continuing volume heating of the lattice due to the energy transfer from the electron component result in formation of a superheated subsurface region in the solid with the subsurface maximum of temperature where $T_{ph}(p) > T_m(P)$, Figs. 1 and 2. According to the works [24], [25], the maximum superheating of aluminum is limited by the value of approximately $1.4T_m(P)$. The collapse of the overheated metastable state takes place in the form of volume melting of the superheated region. We chose the following algorithm of consideration of homogeneous melting based on the above criterion of maximum superheating. When the temperature in some point of solid reaches the value of $1.4T_m(P)$ (this point is shown with an arrow at Fig. 1), a new liquid phase is introduced (a quasi-nuclei). It is represented by two

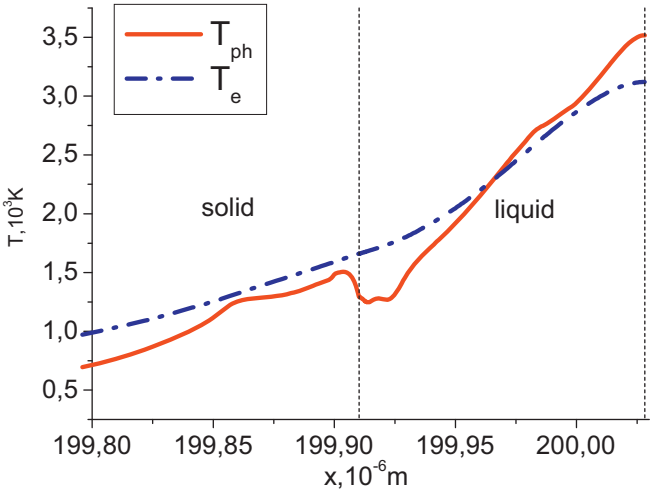

Fig. 2. Temperature profiles at the moment before first spallation at $t = +20$ ps. Red solid and blue dash-dot lines are the temperature of phonons and electrons correspondingly.

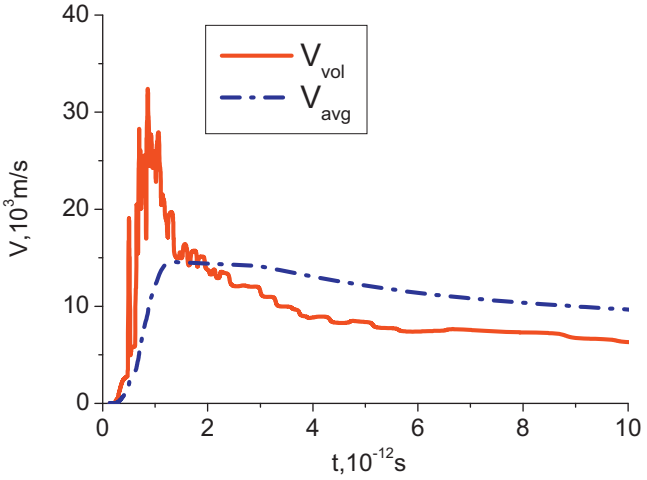

Fig. 3. Time dependence of instant (red solid line) and average (blue dash-dot line) velocity of volume melting. (For interpretation of the references to colour in this figure legend, the reader is referred to the web version of this article).

new melting boundaries, which are introduced with liquid phase between them. They start to move in the opposite directions and that effectively increases the total melting speed i.e., the amount of melted material per second. In this paper, this effective speed is called the speed of homogeneous melting. We write the same boundary conditions at the new boundaries as at the boundary of heterogeneous surface melting. Fig. 3 shows the time dependence of the instantaneous and average speed of a homogeneous melting. Their maximum values are approximately ≈ 32 km/s and ≈ 15 km/s correspondingly. The speeds of homogeneous melting exceed the speed of sound and are much higher than the velocity of the front of heterogeneous melting. The obtained values of the speed of homogeneous melting correlate well with the values for the homogeneous melting of a gold film ≈ 13.2km/s, calculated using the molecular-dynamic approach [26].

The second stage of the development of the processes, t ≥ 0.5ps, is associated with the evolution of the hydrodynamic processes. High speed of the melting front together with the rapid thermal expansion leads to the formation of a strong compression of matter near the melting front. Propagation of the compression wave has a loading effect on the substance and corresponds to the positive half-wave of pressure Fig. 4. The compression stage is followed by a stage of unloading which corresponds to the negative pressure

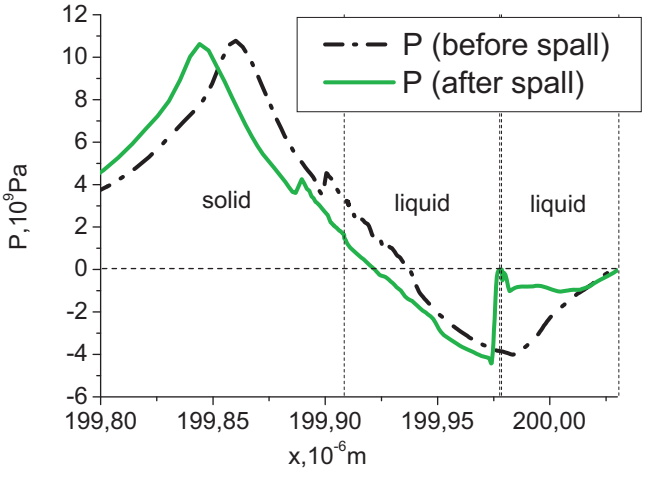

Fig. 4. Pressure profiles at the time instants 1.7 ps before and 0.6 ps after the first spallation (at t = +20.4ps and t = +22.7 ps) correspondingly.

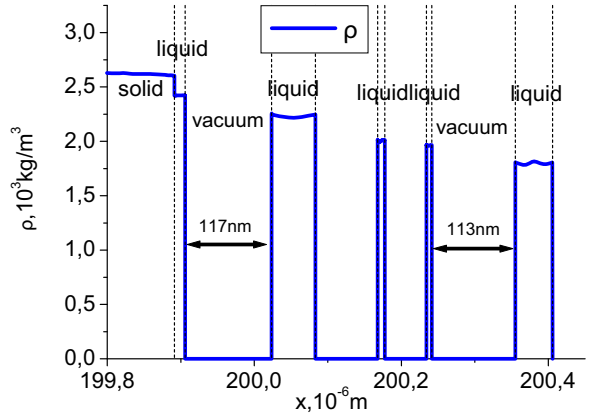

Fig. 5. Density profiles at t = +0.4 ns with 4 spalled parts. Vertical dotted lines show the location of the moving boundaries solid–liquid and vacuum–liquid.

half-wave, Fig. 4. Fig. 4 shows pressure profiles before the first spallation and right after it. Figs. 5 and 6 show the density profiles and electron and phonon temperatures at the moment t = +0.4 *ns*. Four spalled pieces of liquid phase with sizes from 2 to 19 nm are seen at Fig. 5. The total number of spallations in this computation is 20 and some of the spalled parts are later combined with each other and form larger fragments. The total amount of spalled material (calculated based on the mass of solid) is 95 nm. The temperature of the spalled fragments is from 1500 to 2800 K. Multiple passages of pressure waves reflected from the left and right free boundaries are observed in each of the spalled pieces. These waves are most notably seen in the spalled parts with the maximum size, in this calculation they are the very left and very right fragments with the size of 55 and 45 nm, respectively, where the pressure oscillation amplitude reaches the value of 1–2 GPa. The average speed of movement of the very left fragment is about 400 m/s, the speed of the very right one is about 1000 m/s. It should be also noted that the most of the liquid phase in this calculation is spalled after the passage of the rarefaction wave; the size of the remaining non-spalled liquid is 25 nm out of 120 nm of the maximum liquid size, Fig. 7. In some other regimes that we simulated, even larger portion of the liquid phase is removed through spallation. These results are in fairly good agreement with the experiment [3] where the spallation threshold fluence was 0.085 J/cm^2 and the spalled fragments sizes were in the range of 10–50 nm.

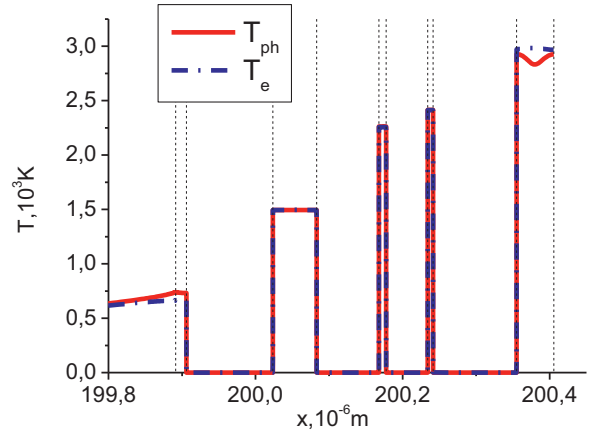

Fig. 6. Phonon (red solid line) and electron (blue dash-dot line) temperature profiles at t = + 0.4 ns. Vertical dotted lines show the location of the moving boundaries solid–liquid and vacuum–liquid. (For interpretation of the references to colour in this figure legend, the reader is referred to the web version of this article).

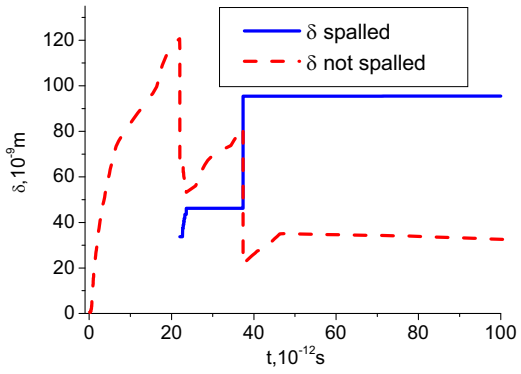

Fig. 7. Not-spalled (red dashed line) and spalled (blue solid line) liquid phase size. (For interpretation of the references to colour in this figure legend, the reader is referred to the web version of this article)

6. Conclusion

The basis of the high-speed laser ablation, which is manifested in the form of a spallation of melt from the side of the irradiated surface, is the interaction of mechanisms of homogeneous and heterogeneous melting. The key point of our suggested approach is explicit tracking of the phase boundaries. The resulting melt is removed in the unloading wave, which corresponds to the negative branch of the pressure, propagating from the surface into the bilk material. The threshold fluence value in our computation is about $F = 0.26\ J/cm^2$ (absorbed $0.06\ J/cm^2$). The amount of spalled material for $F = 0.4 J/cm^2$ is about ~95 nm. As the fluence rises, the number of fragments also rises to 10–15 with large dispersion of the fragment widths ~(1–25) nm. The described mechanism exists in a rather narrow range of fluence values. For $F > 0.7 J/cm^2$, the dominant mechanism is spinodal decomposition of the superheated phase.

Acknowledgement

The research was funded by the Russian Fund of Basic Research, grant nos. 13-07-00597-a, 12-07-00436-a.

References

[1] V.E. Fortov, V.V. Kostin, S. Eliezer, Spallation of metals under laser irradiation, J. Appl. Phys. 70 (1991) 4524–4531.
[2] H. Tamura, T. Kohama, K. Kondo, M. Yoshida, Femtosecond-laser-induced spallation in aluminum, J. Appl. Phys. 89 (2001) 3520–3522.
[3] S. Amoruso, R. Bruzzese, M. Vitiello, N.N. Nedialkov, P.A. Atanasov, Experimental and theoretical investigations of femtosecond laser ablation of aluminum in vacuum, J. Appl. Phys. 98 (2005).
[4] M.E. Povarnitsyn, T.E. Itina, M. Sentis, K.V. Khishchenko, P.R. Levashov, Material decomposition mechanisms in femtosecond laser interactions with metals, Phys. Rev. B 75 (2007) 235414-1–235414-4.
[5] D.S. Ivanov, L.V. Zhigilei, Combined atomistic-continuum modeling of short-pulse laser melting and disintegration of metal films, Phys. Rev. B 68 (2003) 064114.
[6] D. Perez, L.J. Lewis, Molecular-dynamics study of ablation of solids under femtosecond laser pulses, Phys. Rev. B 67 (2003) 184102.
[7] V.V. Stegailov, S.V. Starikov, G.E. Norman, Atomistic simulation of laser ablation of gold: the effect of electronic pressure, AIP Conf. Proc. 1426 (2012) 905.
[8] J.P. Colombier, P. Combis, E. Audouard, R. Stoian, Guiding heat in laser ablation of metals on ultrafast timescales: an adaptive modeling approach on aluminum, New J. Phys. 14 (2012) 013039.
[9] K. Eidmann, J. Meyer-ter-Vehn, T. Schlegel, S. Huller, Hydrodynamic simulation of subpicosecond laser interaction with solid-density matter, Phys. Rev. E 62 (1) (2000) 1202.
[10] E. Lescoute, L. Hallo, D. Hébert, B. Chimier, B. Etchessahar, V.T. Tikhonchuk, Experimental observations and modeling of nanoparticle formation in laser-produced expanding plasma, Phys. Plasmas 15 (2008) 063507.
[11] L.M. Rechiman, F.J. Bonetto, J.M. Rossello, Effect of the Rayleigh–Taylor instability on maximum reachable temperatures in laser-induced bubbles, Phys. Rev. E 86 (2012) 027301–027305.
[12] E.G. Gamaly, The physics of ultra-short laser interaction with solids at non-relativistic intensities, Phys. Rep. 508 (2011) 91–243.
[13] M.E. Povarnitsyn, T.E. Itina, P.R. Levashov, K.V. Khishchenko, Mechanisms of nanoparticle formation by ultra-short laser ablation of metals in liquid environment, Phys. Chem. Chem. Phys. 15 (2013) 3108–3114.
[14] N.A. Inogamov, et al., Two-temperature thermodynamic and kinetic properties of transition metals irradiated by femtosecond lasers, AIP Conf. Proc. 1464 (2012) 593–608.
[15] V.I. Mazhukin, in: I. Peshko (Ed.), Laser Pulses–Theory, Technology, and Applications, InTech, Croatia, 2012, p. 544.
[16] A.V. Mazhukin, V.I. Mazhukin, M.M. Demin, Modeling of femtosecond laser ablation of Al film by laser pulses, Appl. Surf. Sci. 257 (2011) 5443–5446.
[17] C.J. Tymczak, J.R. Ray, Asymmetric crystallization and melting kinetics in sodium: a molecular-dynamics study, Phys. Rev. Lett. 64 (11) (1990) 1278–1281.
[18] K.A. Jackson, Kinetic Processes: Crystal Growth, Diffusion, and Phase Transitions in Materials, Wiley-VCH Verlag GmbH & Co. KGaA, Weinheim, FRG, 2004.
[19] V.I. Mazhukin, A.A. Samokhin, Boundary conditions for gas-dynamical modeling of evaporation processes, Math. Montisnigri 26 (2012) 8–17.
[20] I.V. Lomonosov, Multi-phase equation of state for aluminum, Laser Part. Beams 25 (2007) 567–584.
[21] V.I. Mazhukin, M.M. Demin, A.V. Shapranov, I. Smurov, The method of construction dynamically adapting grids for problems of unstable laminar combustion, Numer. Heat Transfer Part B: Fund. 44 (2003) 387–415.
[22] D.E. Grady, The spall strength of condensed matter, J. Mech. Phys. Solids 36 (1988) 353–384.
[23] V.I. Mazhukin, A.V. Mazhukin, O.N. Koroleva, Optical properties of electron Fermi-gas of metals at arbitrary temperature and frequency, Laser Phys. 19 (2009) 1179–1186.
[24] B. Rethfeld, K. Sokolowski-Tinten, D. von der Linde, S.I. Anisimov, Ultrafast thermal melting of laser-excited solids by homogeneous nucleation, Phys. Rev. B 65 (2002) 092103-1–092103-4.
[25] Q.S. Mei, K. Lu, Melting and superheating of crystalline solids: from bulk to nanocrystals, Prog. Mater. Sci. 52 (2007) 1175–1262.
[26] Yong Gan, J.K. Chen, Nonequilibrium phase change in gold films induced by ultrafast laser heating, Opt. Lett. 37 (2012) 2193–2691.